Adsorption and catalysis on Pt and Pd monolayer-modified Pt single crystal electrodes

Chen, X.

5

Why Pd Surface Does Not Poison by CO During Formic Acid Oxidation?

This chapter is based on:

Chen, X., Granda-Marulanda, L. P., McCrum, I. T., & Koper, M. T. M. In preparation.

Abstract: *Understanding the atomistic details of how the palladium surface is free of CO poisoning during formic acid oxidation is of crucial importance, for palladium has been regarded as a prospective electrocatalyst. However, the underlying mechanism is still ambiguous. Here, the role of the formate intermediate on $Pd_{ML}Pt(111)$ and Pt(111) surfaces for formic acid oxidation has been studied by means of (high-scan-rate) cyclic voltammetry. Our results show that the $Pd_{ML}Pt(111)$ electrode has a four times higher activity towards formic acid oxidation than Pt(111), with a lower onset potential of 0.20 V_{RHE}, compared to 0.40 V_{RHE} on Pt(111), and is free of CO poison formation. A higher coverage of 1/3 ML of formate anion adsorption on $Pd_{ML}Pt(111)$ electrode compared to that of 1/4 ML for Pt(111) as been identified by fast voltammetry. We suggest that the high formate coverage on $Pd_{ML}Pt(111)$ blocks the ensemble site needed for the dehydration reaction of formic acid to adsorbed CO. We also show that carbon dioxide can be reduced to formic acid on the $Pd_{ML}Pt(111)$ electrode from a low potential of -0.29 V_{RHE} but becomes passivated by CO production when applying more negative overpotentials.*

5.1 Introduction

Low-temperature fuel cells consuming organic molecules as fuel have been regarded as a prospective solution to reduce our dependence on traditional fossil fuels[1,2]. Formic acid is one of the fuel candidates to be employed in a so-called direct formic acid fuel cell (DFAFC)[2,3]. The electrocatalytic formic acid oxidation reaction has also been considered as a model reaction for the oxidation of more complex organic molecules[4]. Of all pure metal electrodes, platinum and palladium show the highest formic acid oxidation activity. Formic acid oxidation on Pt surfaces has been studied extensively and the dual-pathway mechanism[5] has been well established by the community[2]. This mechanism assumes that there are two parallel pathways in the reaction scheme. One pathway leads to the desired final product CO_2 at relatively low potentials through a reactive intermediate (presumably some form of adsorbed formate[6]), and another pathway includes a chemical dehydration step leading to adsorbed CO, which acts as a poison blocking the surface and impedes further oxidation of formic acid. The identification of CO as the poisoning intermediate and its role in the oxidation mechanism has been widely accepted[7], but the nature of the reactive intermediate in the direct pathway is still under strong debate. The prominence of the CO poisoning pathway on Pt electrodes renders Pt an unsuitable catalyst for direct formic acid fuel cells and also not ideal for the study of the direct pathway[8,9].

Recent advances in catalyst development have led to the synthesis of Pd-based metal nanoparticles with excellent catalytic properties towards formic acid oxidation[10]. Pd-based catalysts for the electrochemical formic acid oxidation generally display high activity and, remarkably, the absence of CO poison formation. Therefore, Pd electrodes can be used to study the mechanism of the direct pathway without the interference of CO poisoning, and, perhaps more importantly, to understand how CO poisoning can be avoided. However, there have been relatively few mechanistic studies on well-defined Pd surfaces aimed specifically at understanding why Pd surfaces do not poison with CO. This partially arises from the difficulty to prepare Pd single crystals. Epitaxially grown Pd layers on a foreign metal are an interesting alternative, particularly Pt single-crystal surfaces modified by a Pd monolayer[11-17]. The lattice parameters of both metals are close and it has been pointed out that the reactivity of Pd monolayer system is comparable to that of the corresponding Pd single crystal[18].

Palladium-based materials have also emerged as the best catalysts for the reverse reaction, i.e. carbon dioxide electroreduction to formic acid[19-21]. Theoretically, for a two-electron transfer reaction such as the conversion between formic acid and CO_2, reversible catalysts with very low overpotential must exist[22], and palladium-based electrocatalysts seem to approach this ideal situation closely.

This opens up the possibility of using palladium-based catalysts for application in unitized regenerative fuel cells based on carbon dioxide and formic acid. Recent efforts from our group have verified that Pd overlayers deposited on polycrystalline Pt, reduce CO_2 to formic acid and may perform as reversible catalysts[19]. Further, Pd_xPt_{1-x} nanoparticles were applied as bifunctional electrocatalysts for both the CO_2 reduction and formic acid oxidation and showed improved tolerance to CO poisoning and lower overpotentials[23].

In this chapter, we perform systematic electrochemical studies of formic acid oxidation and carbon dioxide reduction on Pd monolayer decorated Pt single crystals and explore the important role played by the involved formate anions on the direct formic acid oxidation pathway. We also study both reactions in comparison to unmodified Pt single crystals. Our studies reveal the crucial role of adsorbed formate anions in inhibiting CO poisoning during the formic acid oxidation. On the other hand, CO poisoning does occur during CO_2 reduction, but only at relatively high overpotential. The understanding that strong anion/formate adsorption on palladium is the main reason for the lack of CO poisoning during formic acid oxidation offers a new important insight in the design of better and more stable catalysts.

5.2 Experimental Section

5.2.1 Electrochemical Measurements

Electrolytes were prepared from ultrapure water (Merck Millipore, 18.2 MΩ cm, TOC<3 ppb) and high-purity reagents (Merck Suprapur, Sigma-Aldrich Trace Select). Before each experiment, the electrolytes were first purged with argon (Air Products, 5.7) for 30 min to remove air from the solution. In the case of CO_2 reduction experiments, the electrolyte was subsequently purged with CO_2 (Linde, 4.5) for at least 30 min to saturate the solution. For CO stripping experiments, the single-crystal electrode was in contact with a CO (Linde 6.0) saturated solution in hanging meniscus configuration at fixed potential of 0.1 V_{RHE} for 30 s, which is sufficient to form a complete monolayer of CO on the electrode. Afterwards, argon was bubbled for 15 min to remove CO from the solution, followed by the CO oxidative stripping experiment.

Cyclic voltammetry measurements were carried out in standard electrochemical cells using a three-electrode assembly at room temperature. All glassware was cleaned in an acidic solution of potassium permanganate overnight, followed by rinsing with an acidic solution of hydrogen peroxide and repetitive rinsing and boiling with ultrapure water. Pt(111) and Pt(100) bead-type electrodes were

used as working electrodes (diameter of 2.27 mm and 3.46 mm, resp.) for cyclic voltammetry, and 10 mm disk-type electrodes were used for online high performance liquid chromatography (HPLC) experiments, resp. Prior to each experiment, the working electrodes were prepared according to the Clavilier method[24]. A platinum wire was used as counter electrode and a reversible hydrogen electrode (RHE), in a separate compartment filled with the same electrolyte, at the same pH as the electrolyte in the electrochemical cell, was employed as the reference electrode. The electrochemical measurements were performed with the single-crystal electrode in the hanging meniscus configuration. The potential was controlled with an Autolab PGSTAT302N potentiostat. The fast-scan cyclic voltammetry experiments were performed using a Bio-Logic SP-300 potentiostat. The current density shown in this chapter represents the measured current normalized to the geometric area of the working electrode.

5.2.2 Preparation of Pd Monolayers on Pt(111) and Pt(100) Single Crystals

The Pd monolayers were prepared using the method similar to the one reported before[18,25]. The freshly prepared Pt(111) and Pt(100) electrodes were immersed into a Pd^{2+} containing solution at 0.85 V_{RHE}, where no Pd deposition occurred, and the potential was continuously cycled between 0.07 and 0.85 V_{RHE} at 50 mV s^{-1}. The amount of palladium on the Pt(111) surface was monitored by following the evolution of the voltammetric peak at 0.23 V_{RHE} (as shown in Figure D.1a), characteristic of the presence of Pd adatoms, whose charge (and current density) depend on the palladium coverage[25]. The scanning tunnelling microscopy (STM) reveals the small monoatomic high Pd islands nucleate on the Pt(111) surface with no noticeable preference of nucleation sites and a full Pd monolayer without detectable holes can be formed after deposition. The STM image shows the presence of an ordered sulphate adlayer with a $(\sqrt{3}\times\sqrt{9})R19.1°$ structure on the Pd monolayer, which is the case for the (111) facet of Pd[26]. Then the Pt(111) electrode was taken from the cell and thoroughly rinsed with ultrapure water before electrochemical measurements. For the Pt(100) electrode, the single crystal was first taken from the cell and immersed in a NO-saturated solution at open circuit. Next, the crystal was thoroughly rinsed with ultrapure water to avoid any contamination from the acidic nitrite solution and was transferred to the electrochemical cell at 0.85 V_{RHE} and the adsorbed NO was reductively stripped. The NO procedure is a kind of electrochemical annealing which leads to a Pt(100) electrode fully covered by a single palladium monolayer[26]. The palladium monolayer was monitored by following the evolution of the voltammetric peaks at 0.17, 0.27 and 0.39 V_{RHE} (as shown in Figure D.1b).

5.2.3 Online High Performance Liquid Chromatography (HPLC)

For online detection of products dissolved in the electrolyte as a function of applied potential, online HPLC was used[27]. While the potential was changed from 0.0 V to the required potential, samples were collected with an open tip positioned close (~10 μm) to the electrode. Sampling was done at a rate of 60 μL min^{-1}, and each sample had a volume of 60 μL. Since the potential was changed at 1 mV s^{-1}, each sample contained the products averaged over a potential change of 60 mV. After voltammetry, these samples were analyzed by HPLC (Prominence HPLC, Shimadzu; Aminex HPX 87-H column, Biorad).

5.3 Results and Discussion

5.3.1 Formic Acid Oxidation

Figure 5.1a shows the blank voltammogram of $Pd_{ML}Pt(111)$ in 0.1 M $HClO_4$, compared to Pt(111). The $Pd_{ML}Pt(111)$ electrode exhibits the same characteristic regions as Pt(111). For Pt(111), these windows correspond to the H adsorption-desorption feature ($0.05<E<0.35$ V_{RHE}), the double layer region ($0.35<E<0.60$ V_{RHE}), and the adsorption-desorption process for OH_{ads} ($0.60<E<0.90$ V_{RHE})[28].

However, as we have shown in Chapter 4, for the $Pd_{ML}Pt(111)$ electrode, these regions correspond to different reactions[29]. The two peaks in the "hydrogen region" of $Pd_{ML}Pt(111)$ involve the replacement of adsorbed H by adsorbed OH (peak at E=0.25 V_{RHE}) and the replacement of adsorbed OH by adsorbed ClO_4^- (peak at E=0.31 V_{RHE}). At higher potential (>0.65 V_{RHE}), the adsorbed perchlorate is replaced by a higher coverage of OH_{ads} or by adsorbed O. The primary reason for the strong difference between $Pd_{ML}Pt(111)$ and Pt(111) surface is the significantly stronger anion and OH adsorption on the $Pd_{ML}Pt(111)$ surface.

In Figure 5.1b, the voltammograms for the oxidation of formic acid on $Pd_{ML}Pt(111)$ and Pt(111) in 0.1 M $HClO_4$ containing 50 mM HCOOH are shown. In perchloric acid, the effect of anion adsorption should be minimal, though we do note that we assume specific perchlorate adsorption on $Pd_{ML}Pt(111)$ above 0.3 V_{RHE} (see previous paragraph). As shown in Figure 5.1b, on the Pt(111) electrode formic acid oxidation starts from 0.35 V_{RHE} along with a peak current of 2.2 mA cm^{-2} during the positive-going scan, with a slightly higher peak current density during the negative-going scan because the CO poison product has been oxidatively stripped at potentials above 0.70 V_{RHE} (as shown in Figure 5.1c). Figure 5.1b also shows the deactivation of the formic acid oxidation on Pt(111)

due to the accumulation of the generated surface adsorbed CO if we cycle to a vertex potential of 0.6 V_{RHE} at which the adsorbed CO is not oxidatively stripped. The formic acid oxidation current decreases fourfold after 12 cycles. These results are conistent with previous results for Pt(111), namely there exists two parallel pathways (direct and CO formation pathway) during the positive-going scan, while the negative-going scan after CO has been oxidatively stripped at high potential is usually chosen as representative for the formic acid oxidation through the direct pathway only[30].

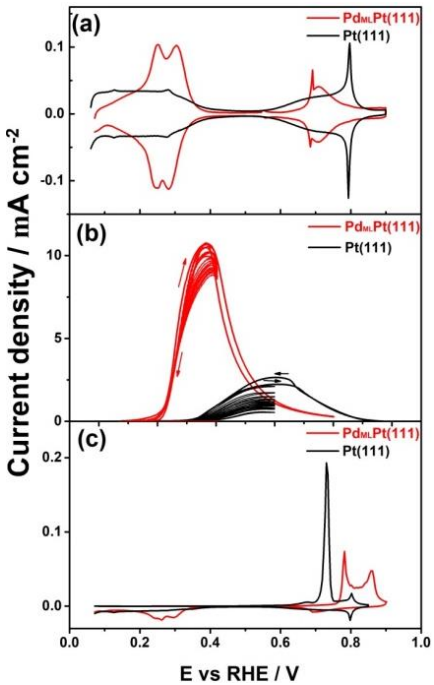

Figure 5.1 (a) Cyclic voltammogram of $Pd_{ML}Pt(111)$ electrode (red) and Pt(111) (black) in 0.1 M $HClO_4$. (b) Voltammograms for the oxidation of formic acid on $Pd_{ML}Pt(111)$ electrode (red) and Pt(111) (black) in 0.1 M $HClO_4$ + 50 mM HCOOH. The evolution of 12 cycles on a rotating $Pd_{ML}Pt(111)$ (red) and Pt(111) (black) electrode at 1600 rpm with continuous cycling to two lower vertex potentials: one to the potential of the oxidation peak where no oxidative stripping of adsorbed CO takes place (see Figure 1c), and one to a higher potential at which adsorbed CO is oxidatively stripped off. Scan rate: 50 mV s^{-1}. (c) CO stripping voltammogram for $Pd_{ML}Pt(111)$ electrode (red curve) and Pt(111) (black curve) in 0.1 M $HClO_4$. Scan rate: 10 mV s^{-1}.

For $Pd_{ML}Pt(111)$ electrode, a peak current density of 11.0 mA cm^{-2} at 0.38 V_{RHE} (ca. four times higher current than on Pt(111), at a 0.2 V lower potential) is observed together with a low onset potential of around 0.20 V_{RHE}. The remarkable observation in Figure 5.1b is that there is hardly any hysteresis for the oxidation current in the positive- and negative-going scan of $Pd_{ML}Pt(111)$ electrode between 0.05 and 0.40 V_{RHE}, suggesting the absence of CO poisoning. Therefore, only the formic acid oxidation direct pathway occurs, in agreement with previous studies[12,14]. Figure 5.1c shows that

surface-adsorbed CO on the $Pd_{ML}Pt(111)$ electrode cannot be oxidatively stripped until the positive-going scan reaches 0.90 $V_{RHE.}$ Comparison of the blank voltammograms of $Pd_{ML}Pt(111)$ and Pt(111) in Figure 5.1a with the formic acid oxidation curves in Figure 5.1b indicates that the onset of formic acid oxidation appears to coincide with hydrogen desorption at 0.20 V_{RHE}, suggesting that the adsorbed hydrogen inhibits the formic acid oxidation.

Figure 5.1c shows the CO stripping voltammograms of $Pd_{ML}Pt(111)$ and Pt(111) surfaces in 0.1 M $HClO_4$, resp. Very low currents are measured on both $Pd_{ML}Pt(111)$ and Pt(111) electrodes during the positive-going scan until 0.6 V_{RHE}, implying that both surfaces are completely blocked by adsorbed CO at low potential. From this observation we conclude that CO binds strongly and irreversibly to both surfaces. For Pt(111), the oxidative stripping peak for adsorbed CO is located at about 0.72 V_{RHE} and the subsequent scan shows the well-known butterfly feature of Pt(111) in 0.1 M $HClO_4$. By comparing to Pt(111), the CO stripping peak of $Pd_{ML}Pt(111)$ electrode is shifted to more positive potentials, between 0.80 and 0.90 V_{RHE}, suggesting slower CO oxidation kinetics on $Pd_{ML}Pt(111)$ compared to Pt(111) under identical experiment conditions, in agreement with a previous report[26]. The charge corresponding to the CO stripping peak is related to the CO coverage, from which we estimate the coverages of CO on Pt(111) and $Pd_{ML}Pt(111)$ electrode to be 0.69 and 0.75 ML, resp., consistent with previous reports for Pt(111)[31,32] and Pd(111)[33]. From these observations, we infer that we cannot ascribe the lack of CO poisoning during formic acid oxidation on $Pd_{ML}Pt(111)$ to a lower CO adsorption strength; if anything, the stripping results show that CO binds stronger to $Pd_{ML}Pt(111)$ than to Pt(111).

5.3.2 Formate Adsorption Isotherm

Given the important role of adsorbed formate in the oxidation mechanism, we want compare the adsorbed formate coverages for Pt(111) and $Pd_{ML}Pt(111)$ as a function of potential. At normal scan rates, the electrochemical signal corresponding to formate adsorption is masked by the formic acid oxidation currents; however, by employing higher scan rates, it is possible to detect adsorbed formate[30]. The current for the reversible formate adsorption/desorption process is proportional to the scan rate, whereas the current for the oxidation of formic acid is independent of the scan rate as this is a process which is purely controlled by the kinetics of the reaction. Thus, by selecting fast enough scan rates, the current corresponding to the adsorption process will be much larger than the current corresponding to the oxidation of the intermediate so that this latter contribution can be considered negligible.

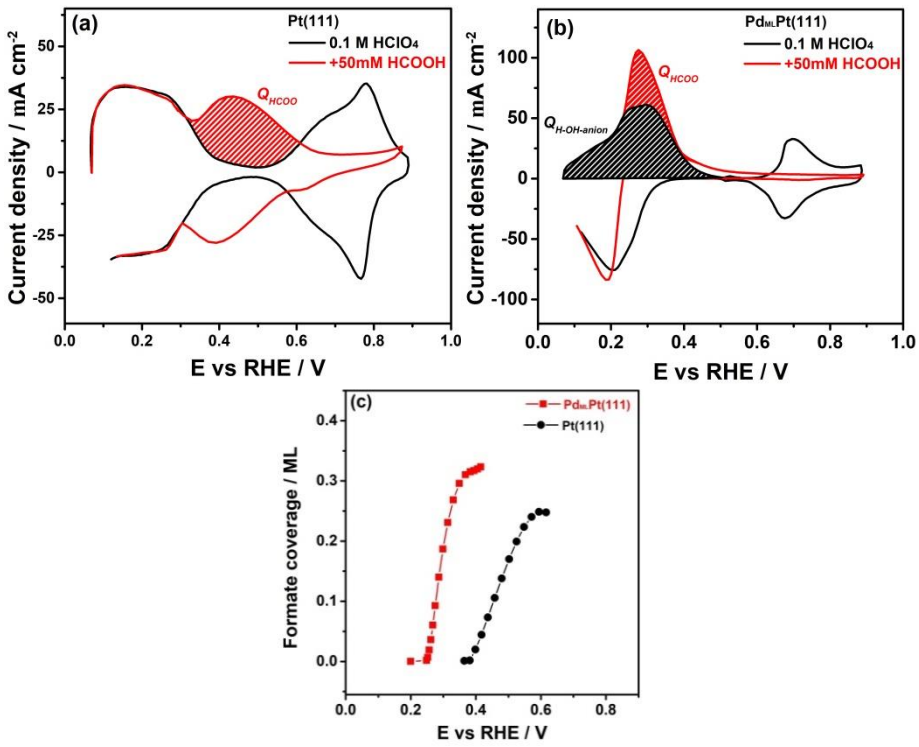

Figure 5.2 Voltammograms of (a) Pt(111) and (b) $Pd_{ML}Pt(111)$ electrode in 0.1 M $HClO_4$ (black line) and 0.1 M $HClO_4$ + 50 mM HCOOH (red line) solution at a high scan rate of 50 V s^{-1}. (c) Comparison between the coverage for the adsorbed formate on the $Pd_{ML}Pt(111)$ and Pt(111) electrode and the formic acid oxidation curve recorded at 50 mV s^{-1}.

Figure D.3a and b show the blank voltammograms of Pt(111) and $Pd_{ML}Pt(111)$ in 0.1 M $HClO_4$ solution recorded at 0.05 and 50 V s^{-1}, resp. As can be seen, the currents associated to the typical H_{upd}, double layer region and OH adsorption profile of the Pt(111) electrode in perchloric acid media recorded at 50 V s^{-1} have increased 3 orders of magnitude in comparison to that of 0.05 V s^{-1}. Although there appears to be a change in shape change in the low potential region (0.05<E<0.40 V_{RHE}) of $Pd_{ML}Pt(111)$ recorded at 50 V s^{-1} compared to the blank at 0.05 V s^{-1}, the charge associated to the H_{upd} and anion adsorption has the same value of 240 μC cm^{-2}. The OH adsorption profile of the $Pd_{ML}Pt(111)$ electrode, between 0.65 and 0.8 V_{RHE}, recorded at 50 V s^{-1} also increases 3 orders of magnitude than that recorded at 0.05 V s^{-1}. In the presence of formic acid, as shown in Figure 5.2a, the high-scan rate voltammogram of Pt(111) is practically symmetric around the *j=0* axis, which indicates that currents are mainly due to adsorption processes and that the contribution from the continuous formic acid oxidation process can be neglected. The characteristic H adsorption-desorption feature between 0.05 and 0.35 V_{RHE} is similar to what is found in 0.1 M $HClO_4$, the signal corresponding to formate adsorption is observed between 0.38 and 0.70 V_{RHE}, whereas the

OH adsorption feature has diminished due to the blocking effect of adsorbed formate, in agreement with previous fast voltammetry results[30]. The potential region of adsorbed formate agrees with that observed by ATR-FTIR on polycrystalline Pt electrodes[34]. Figure 5.2b shows the high scan-rate voltammogram of $Pd_{ML}Pt(111)$ in 0.1 M $HClO_4$ + 50 mM HCOOH. The characteristic H-OH-anion feature between 0.05 and 0.40 V_{RHE} overlaps with the signal corresponding to formate adsorption, whereas the OH/O adsorption feature has diminished due to the formate blocking effect. To determine the charge corresponding to the adsorption of formate (Q_{HCOO}) on the $Pd_{ML}Pt(111)$ electrode, we calculate the charge corresponding to the adsorption states in the presence of formate, and subtract the charge corresponding to the feature H-OH-anion ($Q_{H\text{-}OH\text{-}anion}$) in the absence of formic acid (see Figure 5.2b).

If the double layer capacity of Pt(111) is the same in the absence and presence of formic acid, we can obtain the experimental isotherms for formate absorption on both surfaces from high scan-rate voltammetry, assuming an electrosorption valency equal to -1. According to the spectroscopic studies, the adsorbed formate (HCOO) on the Pt[6,35] and Pd[36,37] surface is bidentate formate. It is now generally agreed that the adsorbed bidentate formate species exist stably on the surface and does not desorb oxidatively as CO_2[7,38,39]. Therefore, the bidentate formate should be considered as a spectator species in the formic acid oxidation pathway. A fully saturated layer of bidentate formate has a coverage of 0.5 ML per Pt surface atom.

Comparing the bidentate formate coverage-electrode potential curves in Figure 5.2c on Pt(111) and $Pd_{ML}Pt(111)$ electrode, the bidentate formate adsorbate reaches a higher coverage of 1/3 ML on $Pd_{ML}Pt(111)$ than that of 1/4 ML on Pt(111). Also, formate binds at ca. 0.2 V lower potential on $Pd_{ML}Pt(111)$, implying stronger adsorption of formate on the palladium-modified surface.

5.3.3 Formate and CO Production From CO_2 Reduction

Next, we turn our attention to a comparison of CO_2 electroreduction on $Pd_{ML}Pt(111)$ and Pt(111). Figure 5.3 shows the production of formic acid and (adsorbed) CO from the reduction of CO_2 on $Pd_{ML}Pt(111)$ (Figure 5.3a) and Pt(111) (Figure 5.3b) electrode as function of potential. The formic acid production was followed with online HPLC as introduced in the Experimental Section. Figure 5.3a shows the production of formic acid on the $Pd_{ML}Pt(111)$ electrode starts at a potential of -0.29 V_{RHE} and approaches a peak production around -0.60 V_{RHE}, and the trend here is similar to our previous results of $Pd_xPt_{(1-x)}$ nanoparticles[19]. Recently reported Pd catalysts also demonstrate formate formation at low overpotential and high efficiency[20]. On the other hand, Pt(111) does not produce any

measurable amounts of formic acid. Previous studies have shown Pt(111)[40] and Pd(111)[41] single crystal electrodes to be inefficient CO_2 electroreduction catalysts as they convert CO_2 to adsorbed CO as the major product.

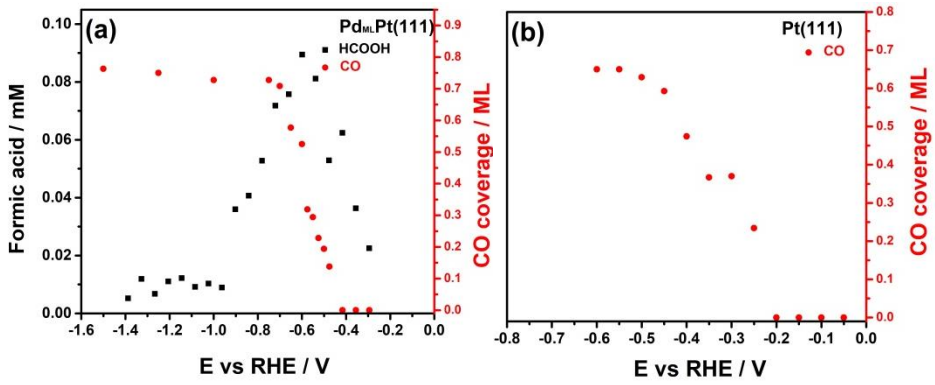

Figure 5.3 Formation of formic acid detected with online HPLC and the CO coverage calculated from stripping voltammograms on (a) $Pd_{ML}Pt(111)$ and (b) Pt(111) electrode under the same experimental condition.

To investigate the formation of CO during CO_2 reduction on the $Pd_{ML}Pt(111)$ and Pt(111) electrode, experiments were carried out by stripping off adsorbed CO by going to positive potentialas shown in Figure D.4a and b. We first scanned the potential to different negative vertex potentials performing CO_2 reduction at 1 mV s^{-1} following the same process as with online HPLC. Next, the electrode was scanned to positive potentials at 10 mV/s, in the same cell immediately after finishing CO_2 reduction to avoid any contamination/exposure to air during electrode transfer. The corresponding cyclic voltammograms are shown in the Supplementary Information. From the CO stripping charges, we can determine the CO surface coverage generated during the CO_2 reduction; these CO coverages are shown as red data points in Figure 5.3.

Figure 5.3 shows that on the $Pd_{ML}Pt(111)$ electrode CO_2 reduction starts producing adsorbed CO at potentials more negative than -0.475 V_{RHE}, whereas on Pt(111) adsorbed CO is formed at potentials more negative than -0.25 V_{RHE}. On $Pd_{ML}Pt(111)$, the CO coverage saturates at ca. -0.70 V_{RHE}. Comparing to the production of formic acid in Figure 5.3a, it is also clear that the formation of formic acid drops as the $Pd_{ML}Pt(111)$ electrode becomes saturated with adsorbed CO. This is thus a clear indication that the $Pd_{ML}Pt(111)$ electrode is able to reduce CO_2 to formic acid at low overpotential window but becomes passivated due to the formation of a CO adlayer when the potential is more negative.

5.3.4 General Discussion

The formic acid oxidation reaction

It is well known that the formation of CO from formic acid requires an ensemble site of two (or more) neighboring free sites[7,42]. The $Pd_{ML}Pt(111)$ shows strong formate adsorption with a high saturation coverage of 1/3 ML. This 1/3 ML formate coverage means that at full coverage 2/3 of the Pd surface atoms are blocked and the ensemble site of two neighboring Pd sites is not accessible. Therefore, CO poisoning is inhibited. The formate in the bulk electrolyte with a configuration of C-H pointing to 1/3 ML of "free" $Pd_{ML}Pt(111)$ surface sites can however react by fast C-H cleavage due to the affinity of the Pd surface to hydrogen. On the other hand, the 1/4 ML saturation coverage of formate on Pt(111) is not high enough to block the ensemble site, and hence the Pt(111) surface becomes poisoned by CO. We are currently studying this model by density functional theory calculations.

The $Pd_{ML}Pt(100)$ electrode shows mass-transport-limited-transport formic acid oxidation at normal scan rate[17]. In order to test our model for this electrode, Figure D.3 shows fast voltammetry results for the formic acid oxidation on $Pd_{ML}Pt(100)$ electrode. Unfortunately, the oxidation of formic acid current on $Pd_{ML}Pt(100)$ electrode in 0.1 M $HClO_4$ + 5 mM HCOOH is very fast, even at 50 V s^{-1}, so that this electrode is too active to determine the saturation coverage of adsorbed formate.

The CO_2 reduction

Pd surfaces produce formate at low potential close to the thermodynamic value of formic acid formation from CO_2 reduction. At more negative potential, the surface passivates due to the accumulation of CO[19,20]. The electrochemically generated surface adsorbed hydrogen has been hypothesized to play a key role during the electrohydrogenation of CO_2 to formate on Pd surface[20]. In this case, high-coverage formate adsorption cannot explain the absence of CO poisoning at low overpotential. We are currently performing DFT calculations to elucidate the origin of the transition from formate to CO production on these electrodes.

5.4 Conclusions

The use of well-defined epitaxially grown Pd monolayers on Pt(111) and Pt(111) single crystal electrodes simplifies the experimental response of surfaces by controlling the surface structure of the electrode and allows unveiling the detailed relationship between surface structure, adsorbed

intermediates, and reactivity. The $Pd_{ML}Pt(111)$ surface shows higher activity for formic oxidation than Pt(111). Most remarkably, the $Pd_{ML}Pt(111)$ surface shows no CO surface poisoning. Our fast-scan voltammetry results show a higher saturation coverage of 1/3 ML formate anions on the $Pd_{ML}Pt(111)$ electrode compared a saturation coverage of 1/4 ML on Pt(111). This high coverage of formate anions blocks the ensemble site necessary for CO formation, explaining why palladium does not poison by CO during formic acid oxidation. On the other hand, during CO_2 reduction, the $Pd_{ML}Pt(111)$ surface produces formate at a low potential of -0.29 V_{RHE} but starts producing adsorbed CO at potentials more negative than -0.475 V_{RHE}. The mechanistic origin of this change in selectivity is currently not fully understood.

References

1 Koper, M. T. M. (Ed.) A. *Fuel cell catalysis: a surface science approach*. (John Wiley & Sons, 2009).
2 Vielstich, W., Lamm, A. & Gasteiger, H. A., *Handbook of fuel cells: fundamentals technology and applications*. Vol. 2 (Wiley New York, 2003).
3 Aslam, N., Masdar, M., Kamarudin, S. & Daud, W. Overview on direct formic acid fuel cells (DFAFCs) as an energy sources. *APCBEE Procedia* **3**, 33-39, (2012).
4 Boronat-Gonzâlez, A., Herrero, E. & Feliu, J. M. Heterogeneous electrocatalysis of formic acid oxidation on platinum single crystal electrodes. *Curr. Opin. Electrochem.* **4**, 26-31 (2017).
5 Capon, A. & Parsons, R. The oxidation of formic acid at noble metal electrodes Part III. Intermediates and mechanism on platinum electrodes. *J. Electroanal. Chem. Interfacial Electrochem.* **45**, 205-231 (1973).
6 Miki, A., Ye, S. & Osawa, M. Surface-enhanced IR absorption on platinum nanoparticles: an application to real-time monitoring of electrocatalytic reactions. *Chem. Commun.* **14**, 1500-1501 (2002).
7 Herrero, E. & Feliu, J. M. Understanding formic acid oxidation mechanism on platinum single crystal electrodes. *Curr. Opin. Electrochem.* **9**, 145-150 (2018).
8 Grozovski, V., Climent, V., Herrero, E. & Feliu, J. M. Intrinsic activity and poisoning rate for HCOOH oxidation at Pt(100) and vicinal surfaces containing monoatomic (111) steps. *ChemPhysChem* **10**, 1922-1926 (2009).
9 Koper, M. T. Structure sensitivity and nanoscale effects in electrocatalysis. *Nanoscale* **3**, 2054-2073 (2011).
10 Jiang, K., Zhang, H.-X., Zou, S. & Cai, W.-B. Electrocatalysis of formic acid on palladium and platinum surfaces: from fundamental mechanisms to fuel cell applications. *Phys. Chem. Chem. Phys.* **16**, 20360-20376 (2014).
11 Kibler, L. A., El-Aziz, A. M., Hoyer, R. & Kolb, D. M. Tuning reaction rates by lateral strain in a palladium monolayer. *Angew. Chem. Int. Ed.* **44**, 2080-2084 (2005).
12 Baldauf, M. & Kolb, D. Formic acid oxidation on ultrathin Pd films on Au(hkl) and Pt(hkl) electrodes. *J. Phys. Chem.* **100**, 11375-11381 (1996).
13 Llorca, M., Feliu, J., Aldaz, A. & Clavilier, J. Formic acid oxidation on Pd_{ad} + Pt(100) and Pd_{ad} + Pt(111) electrodes. *J. Electroanal. Chem.* **376**, 151-160 (1994)..
14 Vidal-Iglesias, F., Solla-Gullon, J., Herrero, E., Aldaz, A. & Feliu, J. Formic acid oxidation on Pd-modified Pt (100) and Pt (111) electrodes: A DEMS study. *J. Appl. Electrochem.* **36**, 1207-1214 (2006).
15 Arenz, M., Stamenkovic, V., Schmidt, T. J., Wandelt, K., Ross, P. & Markovic, N. The electro-oxidation of formic acid on Pt-Pd single crystal bimetallic surfaces. *Phys. Chem. Chem. Phys.* **5**, 4242-4251 (2003).
16 Arenz, M., Stamenkovic, V., Ross, P. & Markovic, N. Surface (electro-) chemistry on Pt (111) modified by a Pseudomorphic Pd monolayer. *Surf. Sci.* **573**, 57-66 (2004).
17 Chen, X. & Koper, M. T. M. Mass-transport-limited oxidation of formic acid on a $Pd_{ML}Pt(100)$ electrode in perchloric acid. *Electrochem. Commun.* **82**, 155-158 (2017).
18 Soriaga, M. P., Stickney, J., Bottomley, L. A. & Kim, Y.-G. *Thin Films: Preparation, Characterization, Applications*. (Springer Science & Business Media, 2002).
19 Kortlever, R., Balemans, C., Kwon, Y. & Koper, M. T. M. Electrochemical CO_2 reduction to formic acid on a Pd-based formic acid oxidation catalyst. *Catal. Today* **244**, 58-62 (2015).
20 Min, X. & Kanan, M. W. Pd-catalyzed electrohydrogenation of carbon dioxide to formate: high mass activity at low overpotential and identification of the deactivation pathway. *J. Am. Chem. Soc.* **137**, 4701-4708 (2015).
21 Chatterjee, S., Griego, C., Hart, J. L., Li, Y., Taheri, M. L., Keith, J. A. & Snyder, J. D. Free Standing Nanoporous Pd Alloys as CO Poisoning Tolerant Electrocatalysts for the Electrochemical Reduction of CO_2 to Formate. *ACS Catal.* **6**, 5290-5301 (2019).
22 Koper, M. T. M. Thermodynamic theory of multi-electron transfer reactions: Implications for electrocatalysis. *J. Electroanal. Chem.* **660**, 254-260 (2011).
23 Kortlever, R., Peters, I., Koper, S. & Koper, M. T. Electrochemical CO_2 reduction to formic acid at low overpotential and with high faradaic efficiency on carbon-supported bimetallic Pd-Pt nanoparticles. *ACS Catal.* **5**, 3916-3923 (2015).
24 Clavilier, J., Armand, D., Sun, S. & Petit, M. Electrochemical adsorption behaviour of platinum stepped surfaces in sulphuric acid solutions. *J. Electroanal. Chem. Interfacial Electrochem.* **205**, 267-277 (1986).

25 Alvarez, B., Berna, A., Rodes, A. & Feliu, J. Electrochemical properties of palladium adlayers on Pt(100) substrates. *Surf. Sci.* **573**, 32-46 (2004).
26 Hoyer, R., Kibler, L. & Kolb, D. The initial stages of palladium deposition onto Pt(111). *Electrochim. Acta* **49**, 63-72 (2003).
27 Kwon, Y. & Koper, M. T. M. Combining voltammetry with HPLC: application to electro-oxidation of glycerol. *Anal. Chem.* **82**, 5420-5424 (2010).
28 Koper, M. T. M. Blank voltammetry of hexagonal surfaces of Pt-group metal electrodes: comparison to density functional theory calculations and ultra-high vacuum experiments on water dissociation. *Electrochim. Acta* **56**, 10645-10651 (2011).
29 Chen, X., Granda-Marulanda, L. P., McCrum, I. T. & Koper, M. T. M. Anion Adsorption on Well-defined Pd Monolayer Deposited Pt(111) Electrode. *Submitted*.
30 Grozovski, V., Vidal-Iglesias, F. J., Herrero, E. & Feliu, J. M. Adsorption of formate and its role as intermediate in formic acid oxidation on platinum electrodes. *ChemPhysChem* **12**, 1641-1644 (2011).
31 López-Cudero, A., Cuesta, A. & Gutiérrez, C. Potential dependence of the saturation CO coverage of Pt electrodes: The origin of the pre-peak in CO-stripping voltammograms. Part 1: Pt(111). *J. Electroanal. Chem.* **579**, 1-12 (2005).
32 Orts, J. M., Fernández-Vega, A., Feliu, J. M., Aldaz, A. & Clavilier, J. Electrochemical behaviour of CO layers formed by solution dosing at open circuit on Pt(111). Voltammetric determination of CO coverages at full hydrogen adsorption blocking in various acid media. *J. Electroanal. Chem.* **327**, 261-278 (1992).
33 Hara, M., Linke, U. & Wandlowski, T. Preparation and electrochemical characterization of palladium single crystal electrodes in 0.1 M H_2SO_4 and $HClO_4$: Part I. Low-index phases. *Electrochim. Acta* **52**, 5733-5748 (2007).
34 Chen, Y. X., Miki, A., Ye, S., Sakai, H. & Osawa, M. Formate, an active intermediate for direct oxidation of methanol on Pt electrode. *J. Am. Chem. Soc.* **125**, 3680-3681 (2003).
35 Samjeské, G., Miki, A., Ye, S. & Osawa, M. Mechanistic Study of Electrocatalytic Oxidation of Formic Acid at Platinum in Acidic Solution by Time-Resolved Surface-Enhanced Infrared Absorption Spectroscopy. *J. Phys. Chem. B* **110**, 16559-16566 (2006).
36 Pronkin, S., Hara, M. & Wandlowski, T. Electrocatalytic properties of Au(111)-Pd quasi-single-crystal film electrodes as probed by ATR-SEIRAS. *Russ. J. Electrochem.* **42**, 1177-1192 (2006).
37 Miyake, H., Okada, T., Samjeské, G. & Osawa, M. Formic acid electrooxidation on Pd in acidic solutions studied by surface-enhanced infrared absorption spectroscopy. *Phys. Chem. Chem. Phys.* **10**, 3662-3669 (2008).
38 Chen, Y. X., Heinen, M., Jusys, Z. & Behm, R. J. Kinetics and mechanism of the electrooxidation of formic acid-spectroelectrochemical studies in a flow cell. *Angew. Chem. Int. Ed.* **45**, 981-985 (2006).
39 Xu, J., Yuan, D., Yang, F., Mei, D., Zhang, Z. & Chen, Y.-X. On the mechanism of the direct pathway for formic acid oxidation at a Pt(111) electrode. *Phys. Chem. Chem. Phys.* **15**, 4367-4376 (2013).
40 Rodes, A., Pastor, E. & Iwasita, T. Structural efects on CO2 reduction at Pt single-crystal electrodes: Part 2. Pt(111) and vicinal surfaces in the [011] zone. *J. Electroanal. Chem.* **373**, 167-175 (1994).
41 Hoshi, N., Noma, M., Suzuki, T. & Hori, Y. Structural effect on the rate of CO_2 reduction on single crystal electrodes of palladium. *J. Electroanal. Chem.* **421**, 15-18 (1997).
42 Cuesta, A., Escudero, M., Lanova, B. & Baltruschat, H. Cyclic voltammetry, FTIRS, and DEMS study of the electrooxidation of carbon monoxide, formic acid, and methanol on cyanide-modified Pt(111) electrodes. *Langmuir* **25**, 6500-6507 (2009).